Development of a Cyclostationary Spectrum Sensing Framework Using Deep Learning Techniques for Cognitive Radio Networks in mmWave Band

Nomfundo Vicky Masuku
Department of Electrical Engineering, Pan African University Institute for Basic Sciences, Technology and Innovation, Nairobi, Kenya
vicky.nomfundo@students.jkuat.ac.ke (corresponding author)

Kibet Langat
Department of Telecommunication and Information Engineering, Jomo Kenyatta University of Agriculture and Technology, Nairobi, Kenya
kibetlp@jkuat.ac.ke

Elijah Mwangi
Faculty of Engineering, University of Nairobi, Nairobi, Kenya
elijah.mwangi@uonbi.ac.ke

Received: 15 February 2026 | Revised: 23 March 2026 and 2 April 2026 | Accepted: 3 April 2026

 DOI: https://doi.org/10.48084/etasr.18193

ABSTRACT

Spectrum sensing is a fundamental component of Dynamic Spectrum Access (DSA) and Cognitive Radio (CR) technology. Accurate and rapid detection of signal presence is essential for the dynamic allocation of spectrum resources to specific devices. This capability is especially important in millimeter-Wave (mmWave) and wideband communication systems. These systems experience significant frequency-selective fading, severe multipath effects, and rapid signal variations over their wide bandwidths; therefore, reliable spectrum sensing methods are required. This paper proposes a spectrum sensing framework based on wavelet-derived cyclostationary feature extraction and a hybrid Convolutional Neural Network–Graph Neural Network (CNN-GNN) model. The extracted wavelet-based cyclostationary features are used to train a Multi-Layer Perceptron (MLP) for nonlinear feature learning. A CNN is trained to learn a time-frequency representation of the signals, whereas the GNN is used to learn both spatial and structural properties of the signals. The proposed model is compared with three different benchmark methods: energy detection, Cyclostationary Feature Detection (CFD) based on the Spectral Correlation Function (SCF), and a CNN-MLP baseline, across multiple evaluation metrics, including the probability of detection (P_d), the probability of false alarm (P_{fa}), Area Under the Curve (AUC), accuracy, and runtime. Simulation results show that the proposed model achieves a P_d above 0.95, an accuracy above 0.95, a P_{fa} below 0.05, and lower runtime than the other methods, demonstrating its effectiveness in supporting DSA and Software-Defined Access (SDA) in mmWave systems.

Keywords-spectrum sensing; Cognitive Radio (CR); Cyclostationary Feature Detection (CFD); Convolutional Neural Network (CNN); Multi-Layer Perceptron (MLP); Graph Neural Network (GNN); probability of detection

I. INTRODUCTION

The need for efficient spectrum utilization has become a primary requirement for ensuring the coexistence of various technologies and services in mmWave frequency bands [1]. This is especially true in the development of new applications like Industrial Internet of Things (IIoT), smart manufacturing, autonomous systems, extended reality, and mission-critical communications, where a large number of devices operate in a geographically constrained environment and require deterministic performance [2, 3]. In this context, Non-Public Networks (NPNs), also known as private 5G networks, represent a key enabler for Industry 4.0 applications by

providing local, reliable, and secure wireless connectivity. NPNs typically operate in shared spectrum or locally licensed spectrum, where the availability of spectrum varies both spatially and temporally as a result of the coexistence of other users. Therefore, mechanisms for dynamic access are required to ensure efficient and interference-aware operation [4-7].

Spectrum sensing represents a central element in enabling DSA by allowing wireless systems to identify the availability of spectrum and detect the presence of incumbent or coexisting transmissions using Cognitive Radios (CRs) [8, 9]. The accuracy of spectrum sensing is especially crucial in millimeter-Wave (mmWave) environments, since channel conditions can change rapidly due to mobility and blockage [10, 11]. While traditional spectrum sensing techniques, such as energy detection, are widely used because of their simplicity and low computational complexity, they suffer from poor performance when the Signal-to-Noise Ratio (SNR) is low, which is a typical condition in mmWave channels. Classical Cyclostationary Feature Detection (CFD) methods are computationally expensive due to the computation of the spectral correlation function and the additional logarithmic complexity introduced by the Fourier transform. Moreover, in mmWave and wideband communication systems, the reliability of CFD decreases as a result of frequency-selective fading, multipath effects, and rapid signal variations across wide bandwidths, which smear and distort cyclostationary features [12, 13]. This is where deep learning provides a powerful alternative approach for reconstructing and learning cyclostationary representations that are not directly observable [14, 15]. An Artificial Intelligence (AI)-enabled low-SNR-optimal spectrum sensing model using neural networks that outperforms classical energy detection was developed in [16]. Authors in [17] developed a Deep Learning and Cyclostationary Feature Detection (DL-CFD) system that simultaneously performs signal classification and jammer identification. Similarly, authors in [18] developed a deep learning-based signal classification in wireless fading channels.

The focus of this research is the development of effective and reliable dynamic spectrum sensing in the mmWave frequency range for environments where the same spectrum is used by multiple users. A cyclostationary spectrum sensing framework using deep learning techniques is presented. While prior works on spectrum sensing rely on either classical cyclostationary analysis or deep learning-based time–frequency methods, they suffer from high computational complexity or lack robustness under low-SNR mmWave conditions.

To address these limitations, the present study makes the following key contributions:

- A novel hybrid spectrum sensing framework that combines wavelet-based cyclostationary feature learning with deep learning models, enabling low-SNR detection without explicit Spectral Correlation Function (SCF) computation and reducing complexity compared to existing methods.
- A signal-aware Convolutional Neural Network (CNN)/Multi-Layer Perceptron (MLP) architecture that integrates cyclostationary inductive bias, reducing the black-box nature of deep learning models while improving robustness under fading and noise compared to CNN-only approaches.
- A Graph Neural Network (GNN)-based cooperative sensing scheme that learns inter-node reliability and spatial correlations, enabling topology-aware fusion beyond traditional CNN/MLP methods.

II. METHODOLOGY

The proposed architecture of the framework is illustrated in Figure 1.

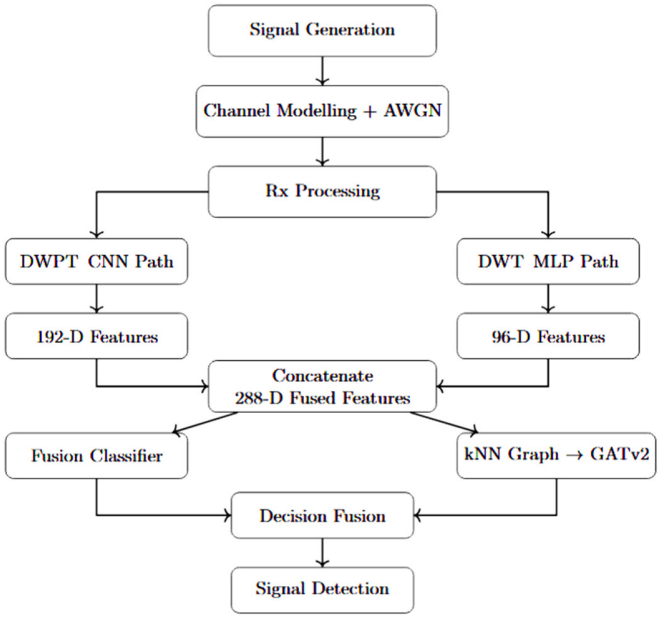

Fig. 1. Flowchart of the proposed CNN-GNN framework.

The spectrum sensing process is modeled as a binary hypothesis test to determine whether a primary user (PU) is currently transmitting in a given frequency band, as shown below:

$$\begin{cases} H_0: x(t) = n(t) & (PU \text{ absent}) \\ H_1: x(t) = s(t) + n(t) & (PU \text{ present}) \end{cases} \quad (1)$$

A. Data Generation

A baseband digital communication signal is generated, starting from a random sequence of bits $b(n) \in \{0,1\}$. The bitstream is grouped into pairs and mapped onto quadrature-modulation (e.g., QPSK, 16-QAM and 64-QAM) symbols, generating a complex-valued baseband symbol stream, $x(n)$, with unit energy per symbol. The Single-Carrier Frequency Division Multiple Access (SC-FDMA) technique is then used to simulate a realistic uplink LTE and 5G transmission environment.

The simulation utilizes a model-based frequency sweep from 30 GHz to 300 GHz, covering the entire lower, middle, and upper mmWave frequency ranges, and extending into the sub-THz regime to evaluate algorithmic robustness and scalability toward beyond-5G scenarios. This sweep allows the dataset to include different path-loss characteristics and

channel behaviors over a variety of frequency-dependent propagation environments.

The transmitted signals pass through a 3GPP TR 38.901 Clustered Delay Line (CDL-A) channel model, with 24 clusters containing 20 rays/cluster. The signal $s_{cp}(n)$ is convolved with the channel impulse response to $H[n,\tau]$, at time n and delay τ. After propagation, Additive White Gaussian Noise (AWGN) is added to the signal over a randomly selected SNR range between –15 dB and +20 dB to test robustness under both low and high SNR conditions. The received signal is therefore given as:

$$y[n] = \sum_{\tau=0}^{L-1} H[n,\tau] \cdot s_{cp}[n-\tau] + w[n] \quad (2)$$

where $w(n)$ is the AWGN and L is the number of multipath clusters in the channel. At the receiver, the received signal $y[n]$ undergoes reverse processing to recover the transmitted time domain symbols, yielding the estimated transmitted symbols $x[n]$.

The dataset is balanced across carrier frequencies and SNR bins by generating absent samples, where the transmitted signal is disabled such that only noise is present at the receiver, ensuring equal representation of signal-present and signal-absent conditions. Table I shows the signal generation parameters.

TABLE I. SIGNAL GENERATION PARAMETERS

Parameter	Description
Sampling rate (F_s)	245.76 MHz
Subcarrier spacing	120 kHz
Number of sub-carriers	1024
Signal bandwidth	122.88 MHz
Symbols per burst	1,024
Cyclic prefix length	64 samples
Channel model	3GPP CDL-A (delay spread = 10 ns, max Doppler = 5 kHz)
Dataset size	10,554 samples (5,277 present, 5,277 absent)

B. Feature Extraction

This stage extracts cyclostationary properties, i.e., repeated patterns in modulated signals that differentiate them from noise, without estimating the cyclic peaks through extensive computations. This is achieved through the application of the Discrete Wavelet Transform (DWT) using a four-stage Haar decomposition on each of the received signals. The DWT enables the capture of cyclostationary signal characteristics via periodic energy distribution across sub-bands, therefore avoiding the computationally intensive cyclic peak estimation process [19]. Figure 2 illustrates the correlation matrix of the fourteen (14) extracted features, showing the inter-feature relationships within the feature set. These extracted features form a 1-D feature map and serve as input to the MLP, with the modulation index feature removed to avoid label leakage.

In parallel with the handcrafted features, each received signal $y[n]$ undergoes a four-level Haar Discrete Wavelet Packet Transform (DWPT), generating a complete set of packet coefficients whose squared magnitudes form a time–frequency packetogram. This 2D map of localized signal energy across time and frequency sub-bands is then resized and normalized to 64 × 64 pixels for input to the CNN.

The MATLAB-generated dataset is imported into Python using a dual-loader capable of handling both standard and HDF5-based .mat formats. For efficient batching and model training, the data are converted into PyTorch tensors. For modeling, a label-stratified split of 80:20 is applied, yielding 8,443 training samples and 2,111 validation samples.

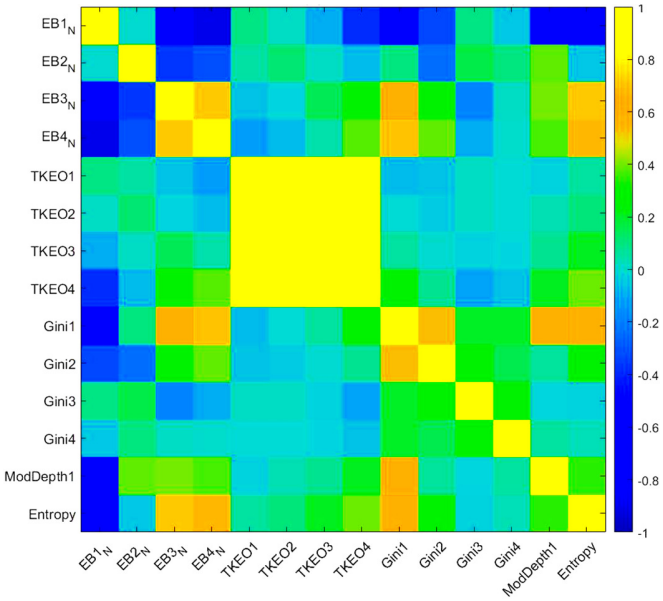

Fig. 2. Correlation matrix of extracted features.

C. Hybrid Model Architecture

The model fuses a lightweight CNN embedding with an MLP embedding and predicts a single binary decision indicating signal presence, as depicted in Figure 1. The dual-branch architecture is motivated by both structural and performance considerations. While the CNN effectively learns hierarchical spatial features from 2D time–frequency representations, it cannot directly process the handcrafted cyclostationary feature vectors, which lack inherent spatial structure. Reshaping these statistical descriptors into a 2D format would impose artificial correlations and compromise their physical meaning. Therefore, an MLP branch is introduced to model these physics-informed features appropriately. The MLP branch operates on the 1D input feature vector $X_{feat} \in \mathbb{R}^{14}$.

The model's prediction is generated by fusing the embeddings from both branches and passing them through a classifier. The feature vectors are combined via concatenation to form a fused feature vector:

$$z = [f_{cnn}; f_{mlp}] \in \mathbb{R}^{192+96} = \mathbb{R}^{288} \quad (5)$$

The fused vector z is then processed by a two-layer multilayer perceptron with ReLU activation and dropout. The output is computed as:

$$o = W^4 \cdot \text{Dropout}(\text{ReLU}(zW^3 + b^3)) + b^4 \quad (6)$$

The final output is an unbounded logit representing the model's raw prediction score obtained by applying the sigmoid function:

$$y = \sigma(o) = \frac{1}{1+e^{-o}} \quad (7)$$

Table II summarizes the hyperparameters used in the CNN-MLP fusion model.

TABLE II. MODEL HYPERPARAMETER SUMMARY

Model	Component	Hyperparameter value
Input	2D time-frequency map	64 × 64 × 1
	1D feature vector	14
	Frame length	1,024 samples per frame
	Normalization method	z-score
CNN branch	Conv1	Filters = 32, kernel = 7 × 7, stride = 1, padding = 3
	MaxPool1	2 × 2, stride = 2
	Conv2	Filters = 64, kernel 3 × 3, padding = 1
	Conv3	Filters = 96, kernel = 3 × 3, padding = 1
	Attention	SE block (r = 8)
	Global pooling	Adaptive AvgPool
	Projection	96 → 192
	Dropout	p = 0.2
	Output embedding	192-dimensional
MLP branch	FC1	14 → 128
	Dropout	p = 0.1
	FC2	128 → 96
	Output embedding	96-dimensional
Fusion classifier	Fusion strategy	Concatenation (192 + 96 = 288)
	FC1	288 → 192
	Dropout	p = 0.3
	Output layer	192 → 1
	Final activation	Sigmoid

D. Semi-Supervised Graph Neural Network

The GNN, as depicted in Figure 3, is a separate standalone post-processing module that leverages relational structures among samples to propagate labels from a small labeled set to a larger unlabeled set. Each node in the graph represents a complete sensing frame (i.e., a time–frequency observation) rather than a frequency bin or spatial sensor. Table III provides the hyperparameters of the GNN network.

The node feature vector is formed by concatenating the fixed embedding extracted from the pre-trained fusion model with contextual metadata, specifically the normalized SNR and a sinusoidal encoding of the carrier frequency. The resulting feature vectors are standardized and reduced to 64 dimensions using Principal Component Analysis (PCA) with whitening. The Graph Attention Network v2 (GATv2) performs message passing to compute a node representation at each layer by aggregating features from its neighborhood.

Under low-SNR and dynamic channel conditions, not all neighboring nodes are equally reliable. Therefore, GATv2 is preferred over the Graph Convolutional Network (GCN), as it adaptively assigns higher attention weights to informative neighbors while suppressing less reliable ones [20].

The semi-supervised nature of the architecture is enforced through a masked loss function. During training, the standard cross-entropy loss is computed only on the labeled subset of nodes. Through backpropagation, the model learns to propagate label information across graph edges from labeled nodes to unlabeled nodes, even though labels for unlabeled nodes are not available during training.

The final system decision is obtained using a logical OR fusion rule. Signal activity is declared when either the real-time classifier or the GNN detects the presence of a primary user.

TABLE III. GNN HYPERPARAMETERS

Component	Hyperparameter
Node feature matrix	Pre-trained fusion embeddings + metadata (PCA-reduced to 64 dimensions, whitened)
Graph construction	k-NN graph (k = 12 nearest neighbors)
GATv2Conv 1	inFeatures = 64, outFeatures = 128, heads = 4, concat = True, dropout = 0.2
Activation	Exponential Linear Unit (ELU)
GATv2Conv 2	inFeatures = 512, outFeatures = 128, heads = 4, concat = True, dropout = 0.2
Output	Softmax (signal present/absent)

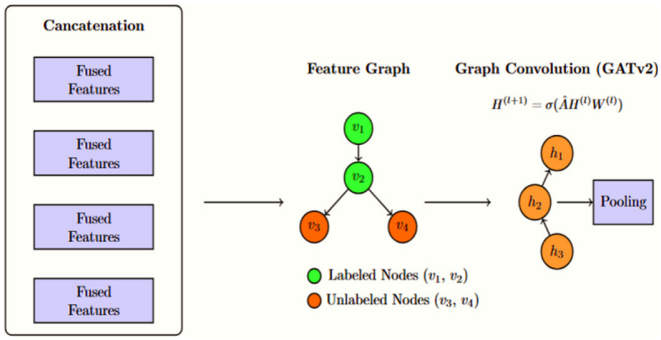

Fig. 3. The GNN architecture.

III. RESULTS AND DISCUSSION

This section discusses the training results and benchmarking performance of the proposed CNN-based model against classical spectrum sensing techniques and deep learning baselines.

A. Training Results

The training log, as presented in Figure 4, demonstrated a stable and well-converged learning process for the fusion model. Across 30 epochs, the training loss decreased steadily from 0.243 to 0.132, whereas the validation loss was improving steadily, showing good generalization. The validation Area Under the Curve (AUC) increased sharply from 0.799 in the first epoch to a maximum of 0.9198, indicating strong discriminative capability between signal presence and absence.

The best model achieved an F1-score of 0.8191 and an accuracy of 0.8257, indicating a good balance between detection sensitivity and false alarm control. Despite minor fluctuations in validation loss, the consistent improvement in AUC and F1-score show that the model has learned meaningful multimodal feature representations and remains robust across a variety of SNR conditions.

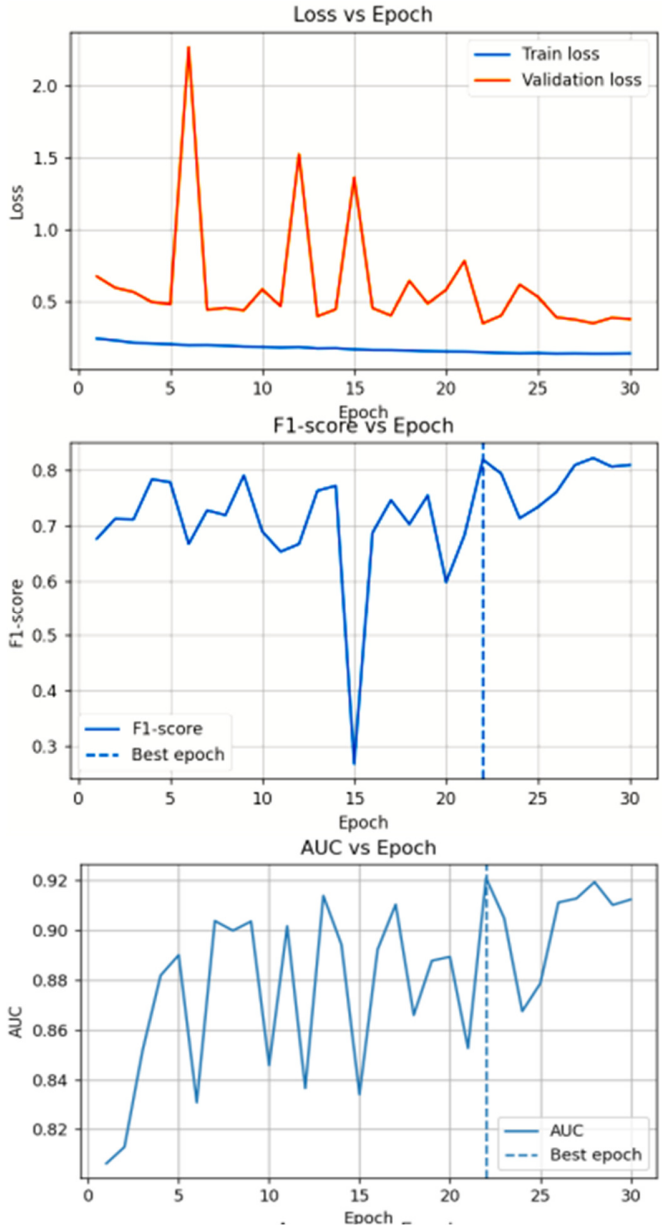

Fig. 4. CNN-MLP training performance.

Overall, the results, as shown in Figure 5, indicate that the fusion classifier successfully generalized to unseen data and achieved high reliability for spectrum occupancy detection. The real-time CNN-MLP classifier operates using the pretrained models, whereas the offline GNN enhances decisions based on its precomputed structural knowledge, providing additional reliability without impacting real-time operation.

The GNN post-training refinement stage achieved an impressive accuracy of 0.9523, an F1-score of 0.9519, and an AUC of 0.957, as shown in Figure 6, representing a substantial improvement over the purely supervised fusion model. This improvement validates that the integration of graph-based relational learning, which links samples via feature-space similarity and utilizes neighborhood information, enhances the classifier's ability to identify low-SNR and boundary cases that are challenging for the fusion model.

In essence, the GNN refinement stage strengthens decision consistency and improves overall detection reliability in challenging propagation environments.

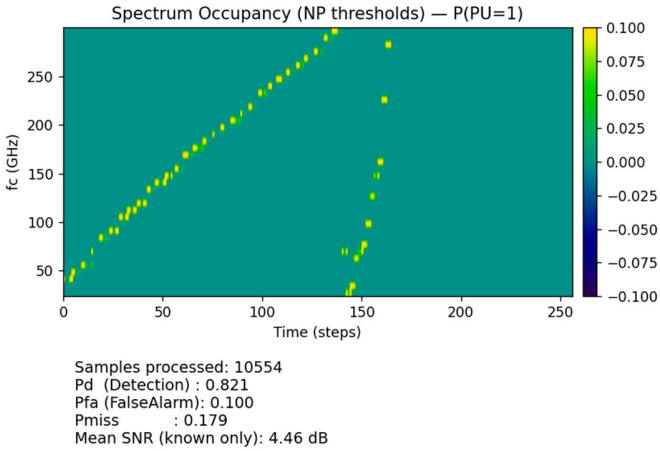

Fig. 5. Real-time dashboard for spectrum occupancy.

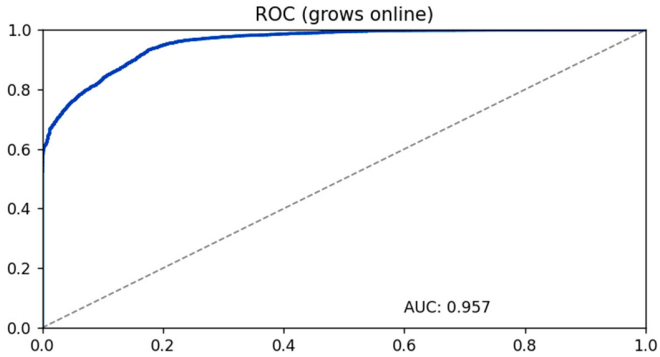

Fig. 6. GNN inference graph.

B. Benchmarking Results

This section provides a comparison of the proposed CNN-GNN spectrum sensing framework against classical and deep learning-based baseline methods. The comparison includes detection performance metrics, robustness to SNR and frequency fluctuations, and computational efficiency. Classical energy detection was implemented using a standard energy-threshold decision rule, whereas CFD was performed using cyclic autocorrelation and spectral correlation analysis to exploit periodic signal structures. The CNN-MLP model represents the proposed deep learning architecture without the GNN component.

All models were evaluated on the same dataset containing 450 signal-present samples and 405 signal-absent samples. The signal-present data were taken from the DeepSense dataset, specifically scenario 36, which contains wideband radio frequency measurement examples representative of actual transmission conditions [21]. Signal-absent samples were generated synthetically by removing the primary-user signal

while maintaining noise and channel characteristics, forming a balanced dataset for sensing evaluation.

The performance summary in Figure 7 clearly shows performance differences between classical and deep learning-based sensing techniques. Energy detection achieved the lowest probability of detection and the highest missed detection rate, demonstrating its sensitivity to noise uncertainty and low-SNR conditions. CFD achieved a zero false alarm rate, indicating strong robustness in distinguishing noise-only samples. The proposed CNN-GNN framework achieved the best overall performance with the highest probability of detection P_d, the lowest probability of missed detection P_{md}, and a significantly reduced probability of false alarm P_{fa} compared to the baseline methods.

```
Performance Summary:
------------------------------------------------------
                Model     Pd     Pfa     PMD Accuracy
    Energy Detection 0.6533 0.1450 0.3467   0.7482
Cyclostationary (SCF) 0.8267 0.0925 0.1733   0.8647
      CNN-MLP (ONNX) 0.9378 0.0700 0.0622   0.9341
    Proposed CNN-GNN 0.9556 0.0469 0.0444   0.9544
```

Fig. 7. Benchmarking results.

The probability of detection versus frequency in Figure 8 shows that CFD exhibits noticeable degradation at higher frequencies due to wideband channel impairments that smear cyclostationary spectral features. Energy detection exhibits rapid degradation in detection probability at low and moderate SNRs, as depicted in Figure 9. In all figures, the CNN-GNN model outperforms the CNN-MLP model, indicating that graph-based cooperative learning enhances robustness by leveraging spatial diversity across sensing nodes.

The Receiver Operating Characteristic (ROC) curves in Figure 10 illustrate the trade-off between detection probability and false alarm rate. The proposed model achieves the highest overall performance, with an AUC of 0.9842, indicating strong discriminative capability across a wide range of thresholds. The CNN-MLP model also demonstrates strong detection performance. CFD provides moderate performance, yet it cannot fully suppress false alarms at lower thresholds. Energy detection exhibits the weakest performance (AUC = 0.6327), with a ROC curve approaching that of a random classifier, reflecting its limited reliability under the tested channel conditions.

The Receiver Operating Characteristic (ROC) curves in Figure 10 illustrate the trade-off between detection probability and false alarm rate. The proposed model achieves the highest overall performance, with an AUC of 0.9842, indicating strong discriminative capability across a wide range of thresholds. The CNN-MLP model also demonstrates strong detection performance. CFD provides moderate performance, yet it cannot fully suppress false alarms at lower thresholds. Energy detection exhibits the weakest performance (AUC = 0.6327), with a ROC curve approaching that of a random classifier, reflecting its limited reliability under the tested channel conditions.

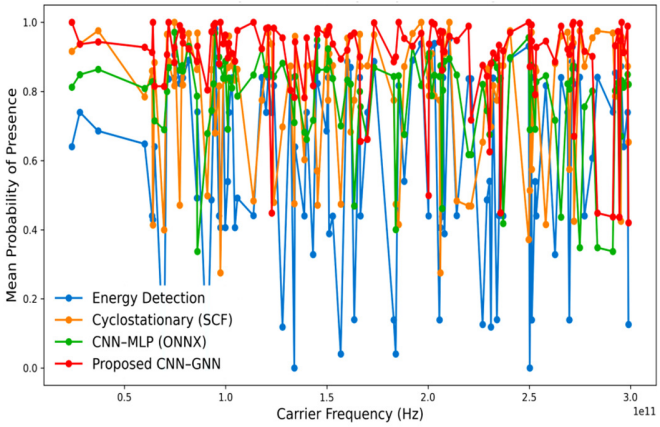

Fig. 8. Probability of detection versus carrier frequency.

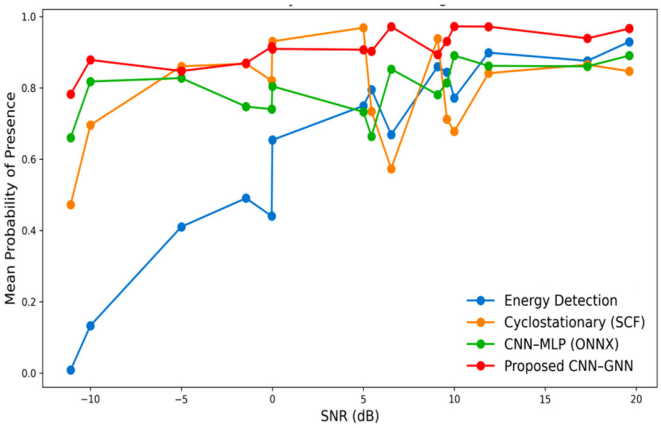

Fig. 9. Probability of detection versus SNR.

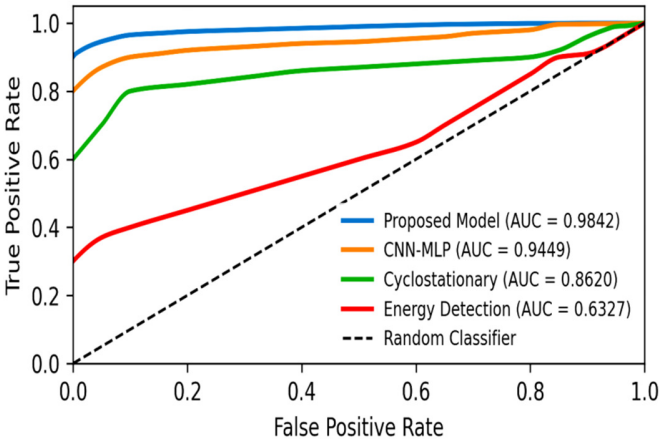

Fig. 10. ROC curves.

The probability density plots in Figure 11 show improved class separability and reduced overlap between the signal-present and signal-absent score distributions compared to the CNN-MLP baseline. This behavior indicates that graph-based relational reasoning reduces uncertainty and improves decision confidence, particularly in low-SNR and frequency-varying conditions.

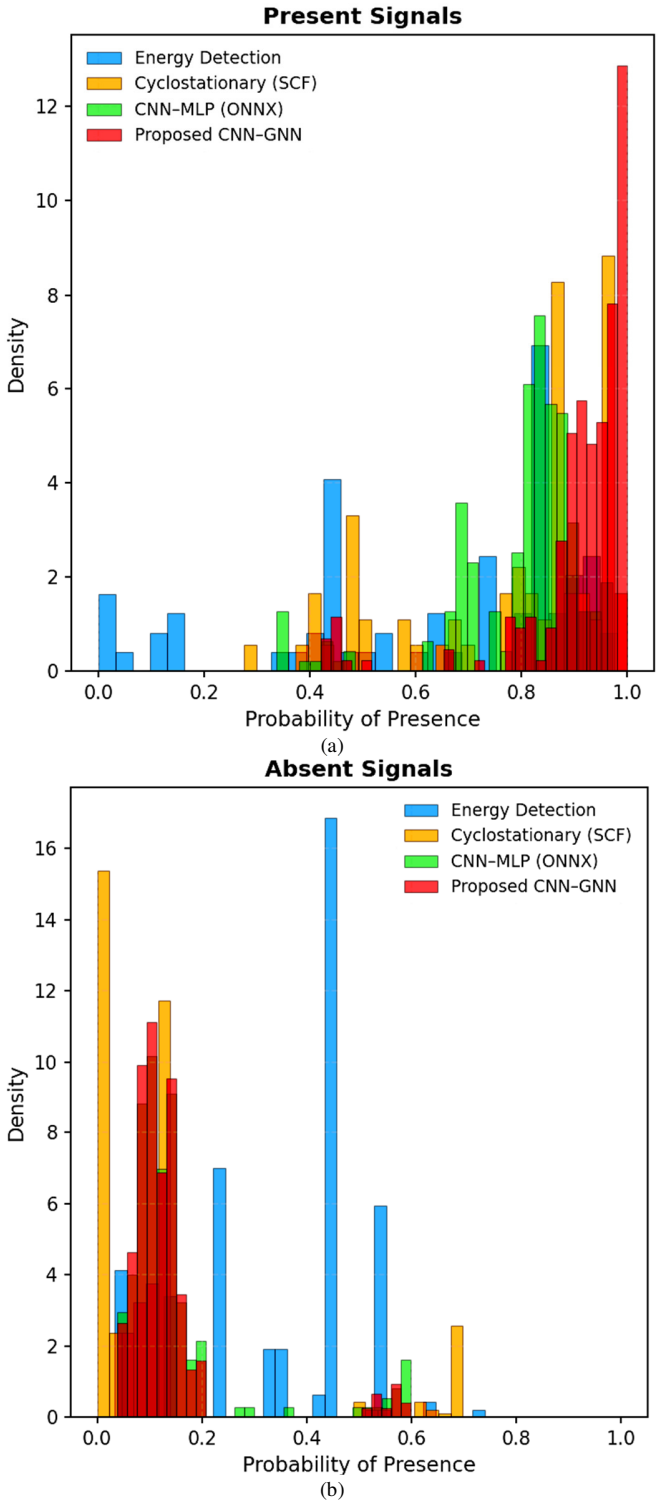

Fig. 11. Probability density functions of predicted signal-presence scores: (a) signal-present samples, (b) signal-absent samples.

The runtime analysis, illustrated in Figure 12, shows that CFD is highly computationally intensive, exhibiting high mean latency and large worst-case runtime. In contrast, energy detection requires 0.58 s of processing time, which is lower than all other methods. Both deep learning models demonstrate significantly shorter and more stable inference times, with the CNN-GNN model incurring only a 0.03 s increase in runtime compared to the CNN-MLP model. This indicates that graph-based reasoning introduces only a marginal computational overhead.

```
================ Runtime Statistics ================
                 Model  Mean (s)  Std (s)  Min (s)    Max (s)
     Energy Detection  0.583782 0.901105 0.000000   4.225016
Cyclostationary (SCF)  3.821055 6.867730 1.956224 141.547680
       CNN-MLP (ONNX)  0.642020 1.566628 0.000000  12.138605
     Proposed CNN-GNN  0.672731 1.208329 0.000000  22.834063
```

Fig. 12. Runtime analysis.

IV. CONCLUSION

Spectrum sensing, enabled by Cognitive Radio (CR) technologies, facilitates the detection of spectrum opportunities and incumbent transmissions, even under challenging conditions characterized by mobility, blockage, and low Signal-to-Noise Ratio (SNR). This capability is increasingly critical with the rapid emergence of applications such as the Industrial Internet of Things (IIoT), smart manufacturing, and Non-Public Networks (NPNs), all of which rely on secure, reliable, and dynamically accessible spectrum resources. In such environments, where spectrum availability is variable and coexistence with incumbent users is required, efficient and adaptive spectrum access mechanisms become essential.

In this work, the Convolutional Neural Network–Graph Neural Network (CNN-GNN)-based spectrum sensing framework demonstrated substantial improvements in detection performance while maintaining low computational cost, with a mean processing time of 0.67 s. Unlike conventional cyclostationary methods, the approach introduces a computationally efficient Cyclostationary Feature Detection (CFD) framework through wavelet-based feature extraction, eliminating the need for explicit Spectral Correlation Function (SCF) computation. Furthermore, unlike purely black-box deep learning models, the framework combines these features with CNN and Multi-Layer Perceptron (MLP) components to preserve interpretability while improving robustness under low-SNR and fading conditions. In addition, a GNN-based cooperative sensing scheme is introduced to learn inter-node reliability and spatial correlations, enabling more effective fusion than traditional methods.

The framework achieves a probability of detection of 0.96, false alarm rates as low as 0.04, and high Area Under the Curve (AUC) performance compared to conventional methods. Extensive simulations using wideband real radio frequency data demonstrate that graph-based cooperative learning improves system robustness under low-SNR and high-frequency conditions, outperforming classical energy detection, CFD, and non-cooperative deep learning baseline methods. With minimal increase in runtime, the proposed method achieves superior detection performance for real-time spectrum sensing applications.

Although the Graph Attention Network v2 (GATv2) is trained offline, this does not compromise operational feasibility. The real-time fusion classifier remains the core decision-making component, meeting latency requirements independently of the GNN. The offline GNN is used only to enhance reliability by combining structural features to improve detection performance. This conservative fusion strategy is designed to protect incumbent users, ensure real-time operation, and improve detection reliability under low-SNR and dynamically changing channel conditions.

Future work will focus on extending the proposed offline framework to real-time GNN-based cooperative inference and on enabling joint detection and classification of multiple modulation schemes, thereby improving spectrum awareness for Cognitive Radio (CR) and millimeter-Wave (mmWave) communication systems.

DECLARATION OF COMPETING INTERESTS

The authors declare that they have no competing interests.

ACKNOWLEDGMENT

The authors wish to express their deepest appreciation to the African Union Organization and the Pan African University Institute for Basic Sciences, Technology and Innovation (PAUSTI) for the financial support that enabled this research. Sincere gratitude is also extended to the Communications Authority of Kenya for institutional support throughout the course of this work.

DATA AVAILABILITY

The dataset used for training the model was generated by the authors and is available from the authors upon reasonable request for academic and research purposes.

REFERENCES

[1] Nidhi, A. Mihovska, and R. Prasad, "Spectrum Sharing and Dynamic Spectrum Management Techniques in 5G and Beyond Networks: A Survey," *Journal of Mobile Multimedia*, vol. 17, no. 1–3, pp. 65–78, Jan. 2021, https://doi.org/10.13052/jmm1550-4646.17133.

[2] J. John, M. Noor-A-Rahim, A. Vijayan, H. V. Poor, and D. Pesch, "Industry 4.0 and Beyond: The Role of 5G, WiFi 7, and Time-Sensitive Networking (TSN) in Enabling Smart Manufacturing," *Future Internet*, vol. 16, no. 9, Sept. 2024, Art. no. 345, https://doi.org/10.3390/fi16090345.

[3] S. I. Loutfi, I. Shayea, U. Tureli, A. A. El-Saleh, and W. Tashan, "An overview of mobility awareness with mobile edge computing over 6G network: Challenges and future research directions," *Results in Engineering*, vol. 23, Sept. 2024, Art. no. 102601, https://doi.org/10.1016/j.rineng.2024.102601.

[4] M. Maman *et al.*, "Beyond private 5G networks: applications, architectures, operator models and technological enablers," *EURASIP Journal on Wireless Communications and Networking*, vol. 2021, no. 1, Dec. 2021, Art. no. 195, https://doi.org/10.1186/s13638-021-02067-2.

[5] A. Aijaz, "Private 5G: The Future of Industrial Wireless," *IEEE Industrial Electronics Magazine*, vol. 14, no. 4, pp. 136–145, Dec. 2020, https://doi.org/10.1109/MIE.2020.3004975.

[6] *Framework and overall objectives of the future development of IMT for 2030 and beyond*, Recommendation ITU-R M.2160-0, International Telecommunication Union Radiocommunication Sector (ITU-R), Geneva, Switzerland, Nov. 2023.

[7] *Service requirements for the 5G system*, 3GPP TS 22.261 V17.10.0, 3rd Generation Partnership Project (3GPP), Sophia Antipolis, France, May 2022.

[8] J. Mitola and G. Q. Maguire, "Cognitive radio: making software radios more personal," *IEEE Personal Communications*, vol. 6, no. 4, pp. 13–18, Aug. 1999, https://doi.org/10.1109/98.788210.

[9] S. Haykin, "Cognitive radio: brain-empowered wireless communications," *IEEE Journal on Selected Areas in Communications*, vol. 23, no. 2, pp. 201–220, Feb. 2005, https://doi.org/10.1109/JSAC.2004.839380.

[10] O. T. H. Alzubaidi, S. Alheejawi, M. N. Hindia, K. Dimyati, and K. A. Noordin, "Interference Mitigation Strategies in Beyond 5G Wireless Systems: A Review," *Electronics*, vol. 14, no. 11, June 2025, Art. no. 2237, https://doi.org/10.3390/electronics14112237.

[11] S. E. Abdelbaset, H. M. Kasem, A. A. Khalaf, A. H. Hussein, and A. A. Kabeel, "Deep Learning-Based Spectrum Sensing for Cognitive Radio Applications," *Sensors*, vol. 24, no. 24, Dec. 2024, Art. no. 7907, https://doi.org/10.3390/s24247907.

[12] A. Kumar *et al.*, "Cyclostationary and energy detection spectrum sensing beyond 5G waveforms," *Electronic Research Archive*, vol. 31, no. 6, pp. 3400–3416, 2023, https://doi.org/10.3934/era.2023172.

[13] M. Nouri, H. Behroozi, N. K. Mallat, and S. A. Aghdam, "A Wideband 5G Cyclostationary Spectrum Sensing Method by Kernel Least Mean Square Algorithm for Cognitive Radio Networks," *IEEE Transactions on Circuits and Systems II: Express Briefs*, vol. 68, no. 7, pp. 2700–2704, July 2021, https://doi.org/10.1109/TCSII.2021.3051087.

[14] A. Xu, "Spectrum sensing based on deep learning with fading channels," M.S. thesis, School of Electrical and Electronic Engineering, Nanyang Technological University, Singapore, 2024.

[15] Y. Zhang and Z. Luo, "A Deep-Learning-Based Method for Spectrum Sensing with Multiple Feature Combination," *Electronics*, vol. 13, no. 14, July 2024, Art. no. 2705, https://doi.org/10.3390/electronics13142705.

[16] M. M. Bhavani, P. Balamurugan, V. N. Sankaran, S. Majumder, Rakshitha. L. P, and K. Nandagopal, "Spectrum Sensing Methodology Using Artificial Intelligence for Cognitive Radio Network," in *2025 First International Conference on Advances in Computer Science, Electrical, Electronics, and Communication Technologies*, Bhimtal, Nainital, India, 2025, pp. 910–914, https://doi.org/10.1109/CE2CT64011.2025.10941172.

[17] T. Nawaz and A. Alzahrani, "Machine-Learning-Assisted Cyclostationary Spectral Analysis for Joint Signal Classification and Jammer Detection at the Physical Layer of Cognitive Radio," *Sensors*, vol. 23, no. 16, Aug. 2023, Art. no. 7144, https://doi.org/10.3390/s23167144.

[18] B. N. Getu, A. Al-Ataby, and H. Attia, "Deep Learning-Based Signal Classification in Wireless Fading Channels," *Engineering, Technology & Applied Science Research*, vol. 15, no. 6, pp. 30296–30303, Dec. 2025, https://doi.org/10.48084/etasr.14585.

[19] M. H. Abood and H. N. Abdullah, "Enhanced Cyclostationary Detector Complexity Based on Haar Wavelet and Signed Correlator," *Mathematical Modelling of Engineering Problems*, vol. 11, no. 7, pp. 1851–1858, June 2024, https://doi.org/10.18280/mmep.110714.

[20] S. Brody, U. Alon, and E. Yahav, "How Attentive are Graph Attention Networks?," in *10th International Conference on Learning Representations*, Virtual Event, 2022, https://doi.org/10.48550/arXiv.2105.14491.

[21] A. Alkhateeb *et al.*, "DeepSense 6G: A Large-Scale Real-World Multi-Modal Sensing and Communication Dataset," *IEEE Communications Magazine*, vol. 61, no. 9, pp. 122–128, Sept. 2023, https://doi.org/10.1109/MCOM.006.2200730.